Simulations of guiding of low-energy ions through a single nanocapillary in insulating materials*

Shi-Dong Liu(刘世东)[1,2], Yong-Tao Zhao(赵永涛)[2,3,†], and Yu-Yu Wang(王瑜玉)[2,‡]

[1] Shandong Provincial Key Laboratory of Laser Polarization and Information Technology, College of Physics and Engineering, Qufu Normal University, Qufu 273165, China
[2] Institute of Modern Physics, Chinese Academy of Sciences, Lanzhou 730000, China
[3] School of Science, Xi'an Jiaotong University, Xi'an 710049, China

(Received 4 May 2017; revised manuscript received 30 June 2017; published online 10 September 2017)

Simulations of guiding of low-energy ions through a single nanocapillary in insulating polymers are reported. The nanocapillary has a diameter of 100 nm and a length of 10 μm. Different from previous work, in our simulations a hyperbolic function is used to describe the decay of the charges deposited on the capillary surface. The present simulations reproduce the self-organized charge-up process occurring in the capillary. It is shown that lower-energy ions undergo more oscillations to get guiding equilibrium than those of higher-energy ions, resulting in a longer charging time, which is in good agreement with previous experimental results. Moreover, the experimentally observed mass independence of ion guiding is proved in our simulations. In particular, it is found that the maximum of the repulsive field within the capillary is independent of the ion energy as well as the tilt angle. To counterbalance the increasing of the transversal energy caused by increasing the tilt angle or incident energy, the effective length of the repulsive field is expanded in a self-organizing manner.

Keywords: ion transmission, capillary guiding, nanocapillary

PACS: 61.85.+p, 34.50.Fa, 72.20.–i **DOI:** 10.1088/1674-1056/26/10/106104

1. Introduction

Over the past decade, the interactions of low-energy ions with the insulating capillaries have been extensively studied. Unlike the phenomena occurring in the metal capillaries,[1] ions can be transmitted along the insulating capillary axis with their initial charge state and incident energy even when the capillaries are tilted by a larger angle with respect to the incident ion-beam direction.[2–5] This phenomenon is called ion guiding, which is attributed to the self-organized formation of charge patches on the capillary internal wall.[2,6]

The guiding process can be qualitatively described as follows: Ions entering into the capillary tilted by an angle hit the wall and, in turn, deposit their charges at the collision points so that a charge patch is generated near the entrance region (hereafter referred as to entrance charge patch). When the entrance charge patch is sufficient to produce a strong repulsive electric field, subsequent ions will be deflected at large distances from the capillary wall. As a result, the close collisions and charge exchanges between ions and atoms on the capillary wall are inhibited. Then, additional small charge patches are formed further inside the capillary.[6–12] Owing to the capillary conductivities, the entrance charge patch is extended and the small charge patches are strongly weakened so that the electric field within the capillary keeps unchanged to maintain ion guiding.[8,11,12]

Experimentally, a large number of researchers have studied the guiding effect using different insulating capillaries[2–6,13–16] accompanied by negative ions,[17–19] molecular ions,[20,21] and electrons,[22,23] as well as various positive ions. Through analysis of various experimental results, many outstanding achievements are acquired. For instance, the observed oscillations of the ion emission angle provide evidence of sequential charge patches formed on the capillary internal wall.[6,24] Particularly, it is found that the guided transmission are not dependent of the ion mass but primarily dependent of the projectile charge-to-energy ratio.[25,26] Recent experiments reported that 1-MeV proton microbeam could be guided through a single cylindrical Teflon macrocapillary,[27] which still needs further interpretations.

Motivated by the desire to understand the guiding mechanisms, theoretical investigations by means of Monte Carlo simulations.[8–12,28] and analytic calculations[29] have been performed in several research groups. These theoretical studies successfully provide more detailed information about ion guiding. It is demonstrated that most of the deposited charges are located near the entrance region.[9–12] To establish ion-guiding equilibrium in simulations, the transport of charges deposited on the capillary wall should be invoked. However, there exist two different models of the charge transport used in previous simulations, namely the drift model[8,11,12] intro-

*Project supported by the National Natural Science Foundation of China (Grant Nos. 11275238, 11205225, and 11375034).
†Corresponding author. E-mail: zhaoyongtao@xjtu.edu.cn
‡Corresponding author. E-mail: wangyuyu@impcas.ac.cn
© 2017 Chinese Physical Society and IOP Publishing Ltd

ducing a nonlinear effect on the charge migration in an electric field, and the diffusion model[9,10] adopting an unbiased random walk to describe the spread and depletion of the deposited charges. Here, it should be pointed out that some general properties of ion guiding can be reproduced by either of these two models. Therefore, a deeper understanding of guiding process within the capillary is still needed. A review on both the experimental measurements and theoretical description of the capillary guiding can be found in Refs. [30] and [31].

The present work is primarily intended to simulate the transmission of ions guided through a nanocapillary and to compare the simulated results with those reported previously. The program is written in MATLAB language which can simplify the procedure codes and improve the developing efficiency greatly. Section 2 describes the simulation methods, inevitably part of which have considerable overlap with those in previous work.[9–11] However, a more justified treatment of the surface-charge decay, which was indicated in early literature,[32–34] is implemented. Section 3 on the simulated results marks the time evolution of the ion transmission, the ion-mass effects on guided transmission, and the electric fields within the nanocapillary. Among the most important finding is that the maximum of the repulsive field is independent of not only the tilt angle but also the ion energy. The summary of the present work is taken up in the final section.

2. Method of ion-guiding simulations

The simulations were designed to explore ion guiding through a cylindrical nanocapillary in polyethylene terephthalate (PET) materials. The nanocapillary has a diameter of 100 nm and a length of 10 μm, whose geometric illustration is shown in Fig. 1 to indicate the coordinate directions.

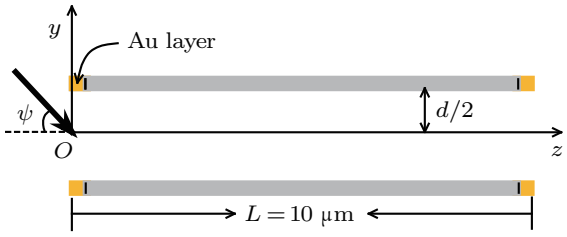


Fig. 1. (color online) The geometric illustration of PET nanocapillary with $d = 100$ nm in diameter and $L = 10$ μm in length (not to scale). The coordinates y and z are indicated in the graph, and the direction of x axis is perpendicular to the paper and points to it (not to show). The ions enter into the capillary with tilt angle ψ relative to the capillary axis, i.e., z axis.

The simulation methods are very similar to those used in Refs. [9]–[12] except for the charge transport caused by the capillary conductivities, so that the overlapped part are outlined briefly. The capillary wall becomes charged due to the deposition of incident ions but without considering the addition charge-up via the secondary electron emission induced by the ion impact with the capillary wall. The trajectories of ions under the function of electric fields produced by the charged wall, are determined by solving Newton's equation of motion. Note that the electric fields are weakened by the image charge of the deposited charges.[35,36] For PET materials with relative permittivity $\varepsilon \simeq 3.2$,[37] the electric fields are reduced by a factor of $(1+\varepsilon)/2 \simeq 2$. Here, it should be pointed out that since we use a single nanocapillary to simulate ion guiding, influences of the capillary neighbors are neglected. Nevertheless, this neglect is justified when the number of capillaries per unit area in foils is not very high.[38]

Due to the capillary conductivities, the charges deposited on the capillary wall will undergo spread and decay, which is key to the guiding process. Since the surface conductivity is much larger than the bulk,[9] only the spread along the capillary surface is taken into account in our simulations. In addition, compared to the drift mechanism, the effect of the diffusion on the charge transport is rather minor.[32] Hence, in our simulations, the diffusion is not invoked.

The spread of deposited charges is considered in terms of the built-in electric field-driven migrations. It is assumed that the charges reaching the golden layer on the front and back surface of the capillary foil will disappear immediately. The carrier mobility governing the charge migration is found to exponentially depend on the square root of the electric field,[39] which is similar to the conductivity modeled by Poole–Frenkel mechanism.[40] To date, it is ambiguous for us whether these two dependencies are exactly within the same framework. Therefore, to avoid the possible inconsistencies, we directly quote the empirical expression for the mobility introduced in Ref. [39], namely,

$$\mu = \mu_0 \exp\left(\sqrt{\frac{|\boldsymbol{E}|}{E_c}}\right). \tag{1}$$

In this expression μ_0 represents the mobility in the field-free case, which is a function of the capillary composition, and $|\boldsymbol{E}|$ is the absolute value of the field. Moreover, the constant field E_c characterizing the exponential increasing of the mobility μ with the field, is defined by

$$E_c = \frac{4\pi\varepsilon_0\varepsilon}{e^2} \cdot \frac{(kT)^2}{e}, \tag{2}$$

where e, T, and k are the elementary charge, the temperature, and the Boltzmann constant, respectively. At room temperature, $E_c \simeq 1.39$ V/μm.

It is obtained from Ref. [41] that the mobility μ_0 of electrons in Mylar (PET) foil is in the neighborhood of 1 nm^2/(V·s). Unlike the treatment of the ion deposition in Ref. [11], we assume that the ion deposited on the capillary wall would become an ion-carrier determining the position of the deposited ion. Accordingly, the mobility for ions is estimated to be smaller than the value of 1 nm^2/(V·s) as a result of the heavy mass. However, as pointed out in Ref. [11],

the mobilities in insulating materials have large uncertainties spanning more than eight orders of magnitude since they are in close relation to the treatment of the internal surface of the hole, such as the humidity, cleanliness.[37,42] Thus, it is unlikely to directly use these mobilities in the simulations. Our methods of determining the mobility is to test the calculations with values varying from 1 $nm^2/V{\cdot}s$ to 10^{-4} $nm^2/V{\cdot}s$, and then find the optimal one by comparing the calculated results to the previous experiments of the capillary guiding. After some tests, it is found that the μ_0 value of 10^{-4} $nm^2/V{\cdot}s$ is appropriate for Ne^{7+}-ion guiding. The test results are presented in Appendix A.

Then, combining the field $\boldsymbol{E}$ with Eq. (1) gives the distance of the ion migration on the capillary surface at the time interval of two incident ions[11]

$$\Delta \boldsymbol{s} = \boldsymbol{E}\mu_0 \frac{q}{I_p d^2} \exp\left(\sqrt{\frac{|\boldsymbol{E}|}{E_c}}\right). \tag{3}$$

Here, q is the charge of the incident ion and I_p is the current density.

Equation (3) is used to determine the positions of charges deposited on the capillary wall. Only when these charges reach the grounded layer, would they be neutralized suddenly. We expect that the number of deposited charges should decrease as they are moving on the capillary wall (see Fig. 2).

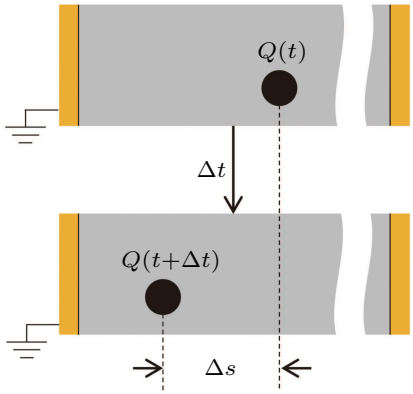


Fig. 2. (color online) The deposited charge $Q(t)$ is changed into $Q(t+\Delta t)$ after a time Δt, and the position is governed by Eq. (3).

In previous simulations,[10,11] the decay of the deposited charge $Q(t)$ is assumed to follow an exponential law to describe the charge diffusion into the capillary bulk. However, as mentioned in Refs. [9]–[12] the bulk conductivity could be neglected compared to the surface conductivity. That is to say, the bulk discharge cannot have a significant impact on guided transmission. Moreover, the guiding experiments[43] exactly claim the charge decay not to be exponential with time. Fortunately, it has been achieved in early studies[32–34] that the charge decay on the insulating surface obeys the following hyperbolic formula:

$$Q(t) = Q_0 \frac{1}{1+t/t_0}. \tag{4}$$

Here, Q_0 represents the initial charges on the surface, and t_0 is a characteristic time constant for which the initial charges decay to 1/2. This formula is obtained based on monitoring the discharge of a charged sample of insulator through a grounded boundary which is similar to the case of the capillary-guiding experiments. Much more information about the derivation of the formula is explained in Refs. [33] and [34]. It has shown a good fit to the experimental data of 3-keV Ne^{7+} ions guided through PET capillaries when the parameter $t_0 \simeq 1000$ s was used.[32] Hence, in our simulations t_0 is fixed at 1000 s to get guiding equilibrium.

Since both equations (3) and (4) are valid within the drift mechanism, one may argue that they give rise to the same charge decay. In order to explain this, we simulate the decay of a uniformly charged square plate in area of 1 μm^2 by using Eq. (3). One side of the plate is grounded. In such simulation, however, the exponential term in Eq. (3) is cancelled (Note that equation (4) was obtained without considering the nonlinear effect). The simulated data, fitted by hyperbolic and exponential functions, is shown in Fig. 3. It is clearly seen that the time evolutions of charges described by Eqs. (3) and (4) are not the same. Besides, it is found from simulations that the charge decay determined by Eq. (3) decreases rapidly at the beginning, and then becomes very slow. This implies that only the charges near the grounded side have a rapid depletion, while those charges far away from the grounded side are difficult to discharge in the way of Eq. (3). Hence, we adopt both of Eqs. (3) and (4) in the simulations. Here, it should be added that from our test calculations the guided transmission cannot be obtained in absence of Eq. (4) (See Appendix A).

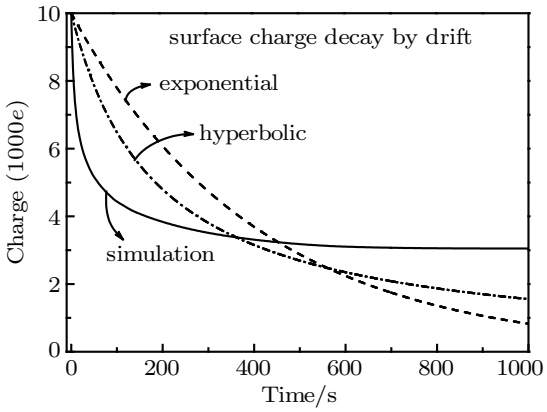


Fig. 3. The decay of a uniformly charged plate simulated by using Eq. (3) without the exponential term. The plate area is 1 μm^2.

The selection of ions and the beam currents, to some extent, is subjective. However, one of the selection criteria is that the ion and the current should be readily available from previous experiments for sake of assessing the precision of our simulations. Besides, on the premise of saving the computing time, the selection is best not to introduce extra approximations and simplifications. Therefore, Ne^{7+} ions with current

of 200 pA/mm^2 is selected, which leads to that the number of Ne^{7+} ions injected into the capillary per second is the equivalent of about 1 with consideration of dielectric screening. To make the simulations more factual , the divergence of incident beam is set to be 0.3° full width at half maximum (FWHM) estimated in previous experiments.[20,44] Here, it is added that we can not explain from first principles why the values of the parameters μ_0 and t_0 should, respectively, be 10^{-4} nm^2/V·s and 1000 s but simply take them as empirical fact that turns out to agree with the experimental observations reported before.

3. Results of simulations

3.1. Ion transmission for different energies

Now, we proceed to the simulations with considering the capillary conductivities. During simulations, the charge migrations on the capillary wall were calculated by Eq. (3), and the charge decay was determined by Eq. (4). We chose 3 keV and 7 keV Ne^{7+} ions as projectiles to compare their temporal properties. The tilt angle is fixed at 2°. The time variations of trajectories for 3-keV and 7-keV Ne^{7+} ions are shown in Fig. 4 together with distributions of charges deposited on the capillary wall.

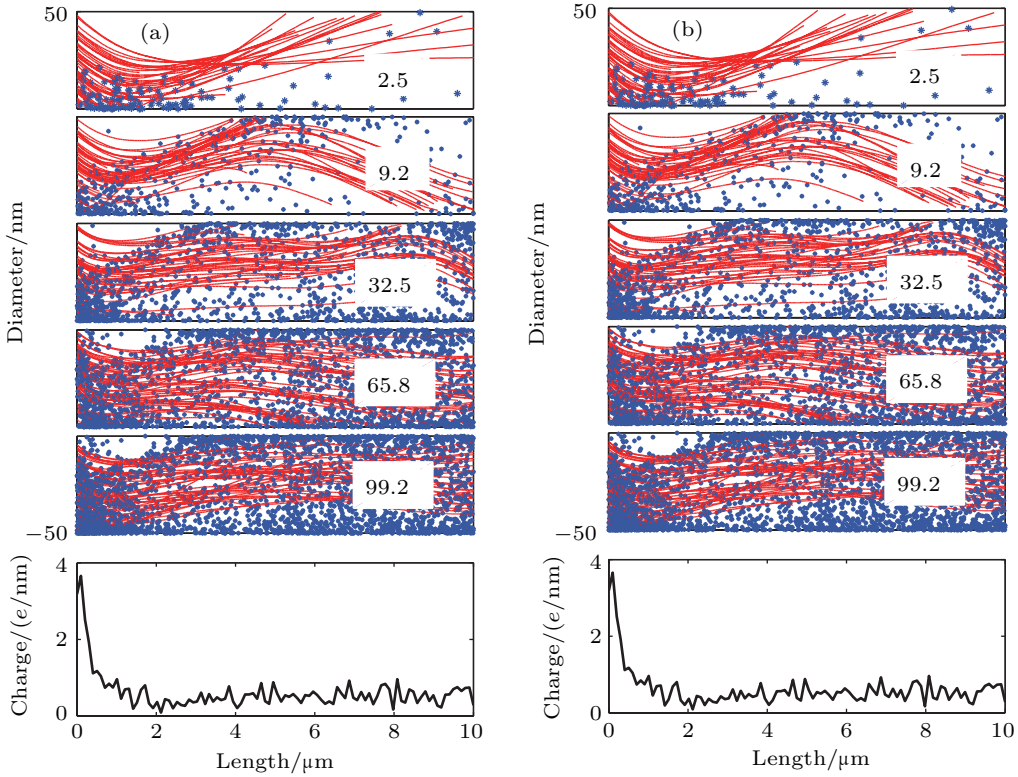


Fig. 4. (color online) Trajectories of 3 keV (a) and 7 keV (b) Ne^{7+} ions and distributions of the deposited charges at guiding equilibrium. The number in each panel indicates the irradiation time (in unit: min).

From Fig. 4, it is clearly seen that the ions undergo oscillatory trajectories before the achievement of the guiding equilibrium, which are caused by the charge patches formed on the back part of the capillary. Due to the discharging via the conductivity, these patches become weaker or nonlocalized so that the ion trajectories will gradually get parallel to the capillary axis. Note that there exists a distinct charge patch near the capillary entrance region from beginning to end (see the bottom panels), which is a general property of the self-organizing mechanism. Similar to the already published results,[11] the entrance charge patch is spread in y-axis direction. This spread is because a certain number of charges are drifted to the wall opposite to the entrance region by the built-in electric field.

Comparing Figs. 4(a) and 4(b), it can be seen that the trajectory oscillations of 3-keV ions are more rapid than those of 7-keV ions, which is in accordance with the experimental observations reported in previous work.[45] Since 3-keV Ne^{7+} ions need less charges to deflect, with the same ion current 3-keV Ne^{7+} ions start deflections faster than 7-keV Ne^{7+} ions. To obtain detailed information about the time evolution of the transmission for 3-keV and 7-keV Ne^{7+} ions, we calculate the transmitted ion fractions as shown in Fig. 5. As proposed in previous work,[2] the transmitted ion fraction can be approximated by the following expression

$$f(t) = f_\infty \left[1 - \exp\left(-\frac{t-\tau_s}{\tau_c}\right)\right], \tag{5}$$

where τ_s is a threshold denoting the time delay for the ion transmission, τ_c is a characteristic time for the capillary charging, and f_∞ represents the fraction at equilibrium. The fitting parameters are given in the graph. Obviously, 3-keV Ne^{7+}

ions need more time to reach a stable transmission than 7-keV Ne^{7+} ions. This is justified since low-energy ions should undergo more deflections to reach stable as suggested in Fig. 4.

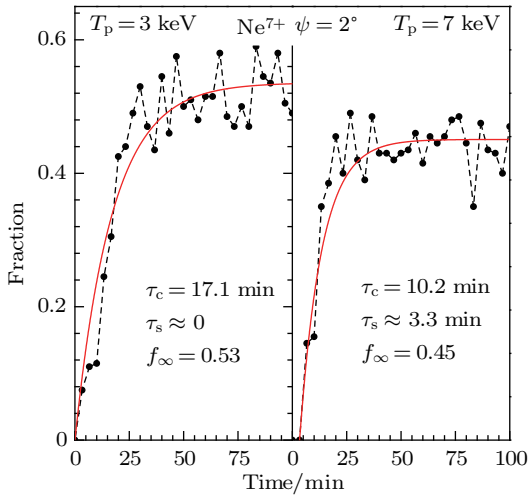


Fig. 5. (color online) Transmission fractions of 3-keV and 7-keV Ne^{7+} ions with tilt angle of 2° as a function of time. The simulated data are fitted by Eq. (5), given as solid lines. The parameters deduced from fits are supplied in the graph.

For comparison of the absolute values of the charging time $\tau_c = 17.1$ min with experiments, a review of the literature was conducted. It was found that for 3-keV Ne^{7+} ions through PET capillaries with 100-nm diameter and 10-μm length tilted by angle of 5°, it needs deposited charge $Q_c \simeq 350$ nC ($Q_c = I_p \cdot \tau_c$) to reach equilibrium.[46] In our simulations, the deposited charge Q_c is about 205 nC (200 pA× 17.1 min), which is reasonable in view of the fact that the tilt angle is not the same. Moreover, various currents also result in different Q_c values.[47]

3.2. Search for ion-mass effects on ion guiding

In order to search the influence of the ion mass on guided transmission, various species of ions were used as projectiles in simulations. Therefore, we studied the fractions of ions transmitted through the nanocapillary. Figure 6 shows the transmission fractions for Ne^{7+}, Ar^{7+}, Kr^{7+}, and Xe^{7+} ions with energy of 7-keV and 1-keV Ne^{1+} ions. These data were acquired for tilt angle of 2°. Here, it should be pointed out that the possible change of the charge state caused by charge-exchange interactions between ions and the capillary wall was not considered in the present simulations. It is seen that all of ion fractions gradually rise after a time delay, and finally reach stable.

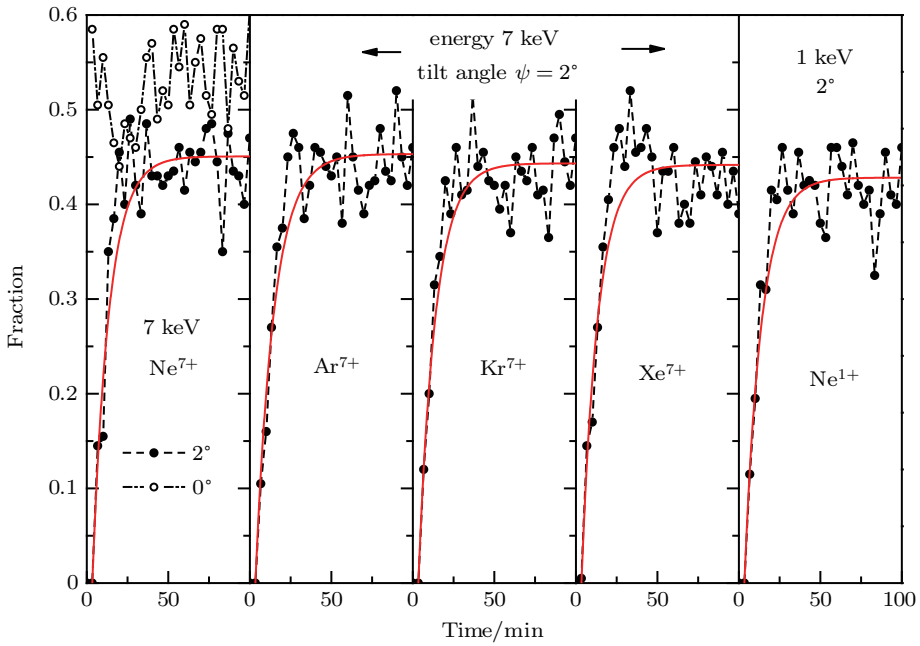


Fig. 6. (color online) Transmitted ion fractions of Ne^{7+}, Ar^{7+}, Kr^{7+}, and Xe^{7+} ions with energy of 7-keV and 1-keV Ne^{1+}. The solid lines represent fits through the simulated data using Eq. (5).

According to the foregoing mention, the time evolution of the ion faction with time is governed by the characteristic time τ_c and the equilibrium faction f_∞ indicated in Eq. (5). Hence, we fitted the data using Eq. (5). The parameters τ_c and f_∞ are summarized in Table 1. The results are found to be nearly equal within uncertainties estimated from the fitting procedure of Eq. (5). The subtle difference among values for various ions comes from the different mass. This finding provides direct evidence that ion guiding though the insulating capillary is nearly independent of ion mass,[25,26] Also, the key parameter governing the guided transmission turns out to be the ratio of the energy to charge. For 2° tilt angle, the equilibrium fraction is about 0.44, while it is about 0.55 at 0°. The value of 0.55 is well comparable to the experimentally measured value of 0.6.[20,44] In consideration of the fractions of 0.27 and 0.12 for 3° and 4°, respectively, we estimated the guiding angle to be

3.2° for $q/T_p = 1$, which is in good agreement with the value of 2.9° predicted by the scaling law.[25]

Table 1. Values of parameters τ_c, τ_s, and f_∞ for different ions.

Energy/keV	Ion	τ_c/min	f_∞
7	Ne^{7+}	10.2 ± 1.4	0.45 ± 0.01
7	Ar^{7+}	11.4 ± 1.5	0.45 ± 0.01
7	Kr^{7+}	10.5 ± 1.4	0.44 ± 0.01
7	Xe^{7+}	10.1 ± 1.5	0.44 ± 0.01
1	Ne^{1+}	10.4 ± 1.4	0.43 ± 0.01

3.3. Field within the nanocapillary

For understanding details of guiding mechanism, we studied the field at guiding equilibrium. It is found that the field component E_x is always zero only with small fluctuations, which implies the symmetric distributions of the deposited charges. Similar to the field E_x, the field component E_z is nearly zero except for that near the capillary entrance. This nonzero E_z whose direction is along the negative z axis, would drift the deposited charges near the capillary entrance to the golden layer and, in turn, gives rise to discharging. Therefore, in the following the attention is focused on the field component E_y which is responsible for the ion deflections within the capillary.

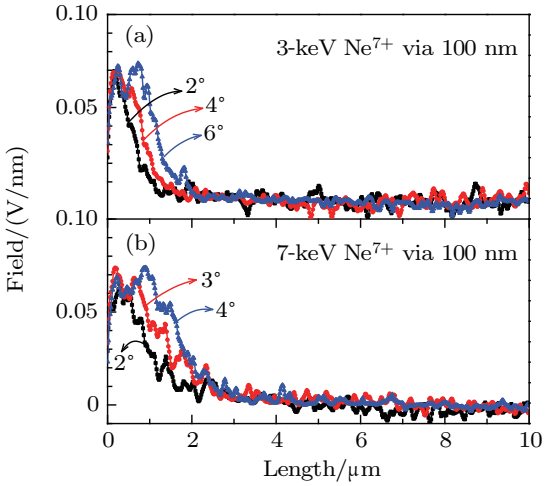


Fig. 7. (color online) The field E_y within the nanocapillary for 3 keV (a) and 7 keV (b) Ne^{7+} ions. These data are calculated at $x = 0$ and $y = 0$ along z axis at guiding equilibrium, i.e., after 100 min irradiation time.

Figure 7 depicts the field E_y for 3-keV and 7-keV Ne^{7+} ions through the nanocapillary with a diameter of 100 nm and a length of 10 μm, as a function of the capillary axis, i.e., z axis. The fields were obtained for tilt angles from 2° to 6° for 3 keV and from 2° to 4° for 7-keV Ne^{7+} ions. It is clearly seen that the maximums of the field component E_y are nearly equal for different nonzero tilt angles. The value is about 0.07 V/nm, which is larger than that ($\sim$ 0.05 V/nm) obtained by Stolterfoht's simulations,[12] but still smaller than the dielectric strength value of about 0.1 V/nm.[25,37] This difference can be attributed to the fact that the diameter of the capillary used in our simulations is half of that in his simulations. The smaller diameter enhances the localization of the entrance charge patch, and in turn, leads to a higher field E_y.

Moreover, the effective length (the part of nonzero values) of the field component E_y increases with the tilt angle, in agreement with previous work.[12] This finding implies that the length of the field should expand in direction of the capillary axis to counterbalance the increasing of the tilt angle. In particular, it is found from comparison of Figs. 7(a) and 7(b) that maximums of the field component E_y are kept unchanged by varying the incident energy. Hence, to guide high-energy ions through the capillary the length of the field component E_y should be extended, as shown in Fig. 7. It appears that the self-expanding of the field E_y is vital for achievements of the ion guiding within the capillary. This finding is interesting in view of the recent experiment[27] that 1-MeV proton microbeam was guided through a cylindrical Teflon macrocapillary.

4. Summary

In summary, the present simulations capture the essential features of the ion transmission guided through the insulating nanocapillary. The simulations indicate that the ions undergo oscillatory trajectories to the exit of the capillary, which result from the several charge patches sequentially formed on the capillary internal surface. Moreover, it needs a longer time for lower-energy ions to get guiding equilibrium as a result of more oscillations, in agreement with the experiments.[45]

On the other hand, the simulations provide direct evidence that the transmission of ions guided through the insulating capillary is nearly independent of ion mass. As expected by the semiempirical scaling law,[25,26] the key controlling parameter of ion guiding is the ratio of charge to energy. This implies that the insulating capillary has pretty promising future in manipulating various charged particles regardless of the mass.

Most importantly, the field component E_y is found to be nearly unchanged by varying the ion energy as well as the tilt angle. Hence, to guide ions with high transversal energy caused by the increasing of the tilt angle or incident energy, the effective length of the field E_y is extended in a self-organized manner.

Appendix A: Test calculations for different mobilities

In the appendix, we show the test results of transmission of 3-keV Ne^{7+} ions through a PET nanocapillary with different values of mobility μ_0. The values are varied from 0 to 1 $nm^2/V{\cdot}s$. Other parameters are set to be the same as those mentioned above unless otherwise stated.

Case 1: $t_0 \to \infty$

Firstly, equation (4) is not included in the test calculations, i.e., $t_0 \to \infty$. Figure A1 shows the transmitted ion fractions for mobilities from 0 to 1 nm^2/V·s. Under these conditions, no satisfactory transmission was achieved. In the case of $\mu_0 = 0$, 0.1, and 1 nm^2/V·s, there is one peak in the transmission curve, while there are a couple of peaks for mobilities from 10^{-4} nm^2/V·s to 10^{-2} nm^2/V·s. Non-single peak is generated by a couple of charge patches formed subsequently on the capillary wall.

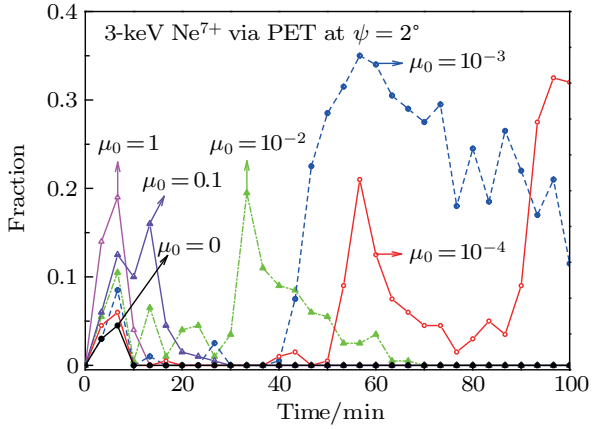


Fig. A1. (color online) The fractions of 3-keV Ne^{7+} ions transmitted through a PET nanocapillary for different mobilities. The data were obtained in absence of Eq. (4).

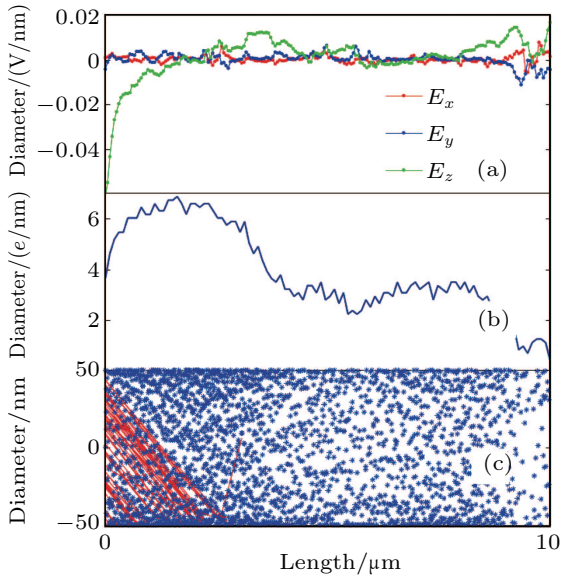


Fig. A2. (color online) The field within the capillary (a), charge density along the capillary axis (b), and the charge distribution on the capillary wall for $\mu_0 = 0.01$ nm^2/V·s at 100 min.

Apparently, for $\mu_0 = 0$ it is due to the strong field created by the over-charged patch to block the ion transmission. However, the capillary is field free in the case of $\mu_0 = 0.1$ nm^2/V·s and 1 nm^2/V·s after 30 min. Note that there is also no repulsive field in the capillary after 70 min for $\mu_0 = 10^{-2}$ nm^2/V·s so that the ion transmission becomes zero, as shown in Fig. A2(a). From comparison between Figs. A2 and A4 we conclude that the field-free capillary is primarily due to the drift of deposited charges toward the opposite side of the capillary wall, rather than dissipation (or neutralization).

Case 2: $t_0 = 1000$ s

Since the transmission is not satisfactory in absence of Eq. (4), the hyperbolic function is then included in our simulations. Here, t_0 is set to be 1000 s according to Ref. [32]. The test results of the transmitted ion fractions are presented in Fig. A3. It can be seen that the transmission is blocked for mobilities higher than 0.01 nm^2/V·s. For $\mu_0 = 10^{-3}$ nm^2/V·s, it needs about 11 min ($Q_c \simeq 130$ nC) to reach guiding equilibrium. Compared to the experimental results reported previously,[46,47] this time seems too small so that we adopt the value of 10^{-4} nm^2/V·s in our simulations.

From our test, it can be concluded that equation (4) plays a vital role in discharging, while equation (3) is mainly responsible for the charge motion in the direction perpendicular to the capillary axis.

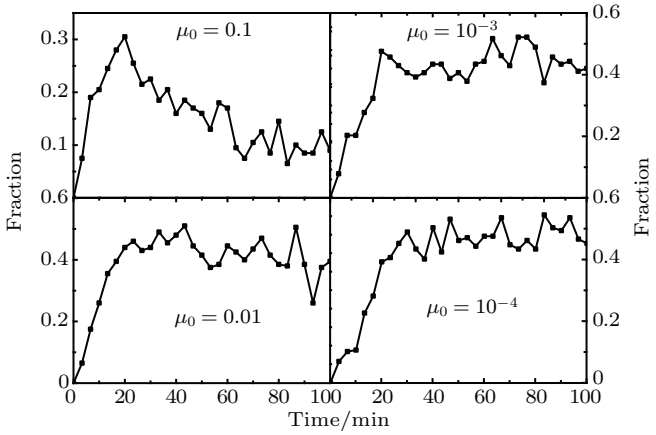


Fig. A3. The fractions of 3-keV Ne^{7+} ions transmitted through a PET nanocapillary. The data were calculated using various mobilities (in unit: nm^2/V·s) indicated in the graph associated with $t_0 = 1000$ s.

Acknowledgment

We thank N Stolterfoht for several helpful discussions on the simulation methods.

References

[1] Ninomiya S, Yamazaki Y, Koike F, Masuda H, Azuma T, Komaki K, Kuroki K and Sekiguchi M 1997 *Phys. Rev. Lett.* **78** 4557
[2] Stolterfoht N, Bremer J H, Hoffmann V, Hellhammer R, Fink D, Petrov A and Sulik B 2002 *Phys. Rev. Lett.* **88** 133201
[3] Víkor Gy, Rajendra Kumar R T, Pešič Z D, Stolterfoht N and Schuch R 2005 *Nucl. Instrum. Methods Phys. Res. B* **233** 218
[4] Sahana M B, Skog P, Víkor Gy, Rajendra Kumar R T and Schuch R 2006 *Phys. Rev. A* **73** 040901
[5] Mátéfi-Tempfli S, Mátéfi-Tempfli M, Piraux L, Juhász Z, Biri S, Fekete É, Iván I, Gáll F, Sulik B, Víkor Gy, Pálinkás J and Stolterfoht N 2006 *Nanotechnology* **17** 3915
[6] Skog P, Zhang H Q and Schuch R 2008 *Phys. Rev. Lett.* **101** 223202
[7] Stolterfoht N, Hellhammer R, Fink D, Sulik B, Juhász Z, Bodewits E, Dang H M and Hoekstra R 2009 *Phys. Rev. A* **79** 022901

[8] Pokhil G P and Cherdyntsev V V 2013 *Journal of Surface Investigation: X-ray, Synchrotron and Neutron Techniques* **7** 356

[9] Schiessl K, Palfinger W, Tökési K, Nowotny H, Lemell C and Burgdörfer J 2005 *Phys. Rev. A* **72** 062902

[10] Schiessl K, Palfinger W, Lemell C and Burgdörfer J 2005 *Nucl. Instrum. Methods Phys. Res. B* **232** 228

[11] Stolterfoht N 2013 *Phys. Rev. A* **87** 012902

[12] Stolterfoht N 2013 *Phys. Rev. A* **87** 032901

[13] Li D H, Wang Y Y, Zhao Y T, Xiao G Q, Zhao D, Xu Z F and Li F L 2009 *Nucl. Instrum. Methods Phys. Res. B* **267** 469

[14] Allen F I, Persaud A, Park S J, Minor A, Sakurai M, Schneider D H and Schenkel T 2006 *Nucl. Instrum. Methods Phys. Res. B* **244** 323

[15] Ikeda T, Kanai Y, Kojima T M, Iwai Y, Kambara T, Yamazakic Y, Hoshino M, Nebiki T and Narusawa T 2006 *Appl. Phys. Lett.* **89** 163502

[16] Xue Y L, Yu D Y, Liu J L, Wu Y H, Zhang M W, Chen J, Wang W, Lu R C, Shao C J, Kang L, Li J Y, Cai X H and Stolterfoht N 2015 *Nucl. Instrum. Methods Phys. Res. B* **359** 44

[17] Feng D, Shao J X, Zhao L, Ji M C, Zou X R, Wang G Y, Ma Y L, Zhou W, Zhou H, Li Y, Zhou M and Chen X M 2012 *Phys. Rev. A* **85** 064901

[18] Chen L, Lü X, Jia J, Ji M, Zhou P, Sun G, Wang J, Chen Y, Xi F, Cui Y, Shao J, Qiu X, Guo Y and Chen X 2011 *J. Phys. B: At. Mol. Opt. Phys.* **44** 045203

[19] Lü X Y, Chen L, Chen X M, Jia J J, Zhou P, Zhou C L, Qiu X Y, Shao J X, Cui Y, Yin Y Z, Wang H W and Ji M C 2011 *Chin. Phys. B* **20** 013401

[20] Stolterfoht N, Hellhammer R, Sobocinski P, Pešića Z D, Bundesmann J, Sulik B, Shah M B, Dunn K, Pedregosa J and McCullough R W 2005 *Nucl. Instrum. Methods Phys. Res. B* **235** 460

[21] Liu S D, Wang Y Y, Zhao Y T, Zhou X M, Cheng R, Lei Y, Sun Y B, Ren J R, Duan J L, Liu J, Xu H S and Xiao G Q 2015 *Phys. Rev. A* **91** 012714

[22] Milosavljević A R, Víkor Gy, Pešić Z D, Kolarž P, Šević D and Marinković B P 2007 *Phys. Rev. A* **75** 030901

[23] Xue Y, Yu D, Liu J, Zhang M, Yang B, Zhang Y and Cai X 2015 *Appl. Phys. Lett.* **107** 254102

[24] Fürsatz M, Meissl W, Pleschko S, Gebeshuber I C, Stolterfoht N, Winter H P and Aumayr F 2007 *J. Phys.: Conf. Ser.* **58** 319

[25] Stolterfoht N, Hellhammer R, Juhász Z, Sulik B, Bayer V, Trautmann C, Bodewits E, de Nijs A J, Dang H M and Hoekstra R 2009 *Phys. Rev. A* **79** 042902

[26] Stolterfoht N, Hellhammer R, Bundesmann J and Fink D 2008 *Phys. Rev. A* **77** 032905

[27] Rajta I, Nagy G U L, Bereczky R J and Tökési K 2015 *Nucl. Instrum. Methods Phys. Res. B* **354** 328

[28] Wang G Y, Shao J X, Song Q, Mo D, Yang A X, Ma X, Zhou W, Cui Y, Li Y, Liu Z L and Chen X M 2015 *Sci. Rep.* **5** 15169

[29] Liu S D, Zhao Y T, Wang Y Y, Stolterfoht N, Cheng R, Zhou X M, Xu H S and Xiao G Q 2015 *Chin. Phys. B* **24** 086104

[30] Lemell C, Burgdörfer J and Aumayr F 2013 *Prog. Surf. Sci.* **88** 237

[31] Stolterfoht N and Yamazaki Y 2016 *Phys. Rep.* **629** 1

[32] Pokhil G P and Vokhmyanina K A 2008 *Journal of Surface Investigation: X-ray, Synchrotron and Neutron Techniques* **2** 273

[33] Liesegang J, Senn B C and Smith E R 1995 *J. Appl. Phys.* **77** 5782

[34] Liesegang J and Senn B C 1996 *J. Appl. Phys.* **80** 6336

[35] Schiessl K, Lemell C, Tökési K and Burgdörfer J 2009 *J. Phys.: Conf. Ser.* **163** 012081

[36] Schiessl K, Lemell C, Tökési K and Burgdörfer J 2009 *J. Phys.: Conf. Ser.* **194** 012069

[37] Electrical Properties of Mylar (http://usa.dupontteijinfilms.com).

[38] Stolterfoht N, Hellhammer H, Sulik B, Juhász Z, Bayer V, Trautmann C, Bodewits E, Reitsma G and Hoekstra R 2013 *Phys. Rev. A* **88** 032902

[39] Gill W D 1972 *J. Appl. Phys.* **43** 5033

[40] Frenkel J 1938 *Phys. Rev.* **54** 647

[41] John C Schug, Lilly A C, Jr and Lowitz D A 1970 *Phys. Rev. B* **1** 4811

[42] Seanor D A 1982 *Electrical Properties of Polymers* (America: Academic Press)

[43] Stolterfoht N, Hellhammer R, Pešić Z D, Hoffmanna V, Bundesmanna J, Petrova A, Finka D and Sulik B 2004 *Vacuum* **73** 31

[44] Hellhammer R, Sobocinski P, Pešić Z D, Bundesmann J, Fink D and Stolterfoht N 2005 *Nucl. Instrum. Methods Phys. Res. B* **232** 235

[45] Kanai Y, Hoshino M, Kambara T, Ikeda T, Hellhammer R, Stolterfoht N and Yamazaki Y 2009 *Phys. Rev. A* **79** 012711

[46] Stolterfoht N, Hellhammer R, Juhász Z, Sulik B, Bodewits E, Dang H M and Hoekstra R 2010 *Phys. Rev. A* **82** 052902

[47] Hellhammer R, Bundesmann J, Fink D and Stolterfoht N 2007 *Nucl. Instrum. Methods Phys. Res. B* **258** 159